The gut microbiota may drive the radiosensitising effect of a high fibre diet

Chee Kin Then#, Salome Paillas#, Alix Hampson, Anne E Kiltie*

CRUK/MRC Oxford Institute for Radiation Oncology, Department of Oncology, University of Oxford

Chee Kin Then chee.then@balliol.ox.ac.uk

Salome Paillas Salome.paillas@oncology.ox.ac.uk

Alix Hampson alix.hampson@oncology.ox.ac.uk

Anne E Kiltie anne.kiltie@oncology.ox.ac.uk

#These authors contributed equally to this work.

*Corresponding author:

Professor Anne E Kiltie

CRUK/MRC Oxford Institute for Radiation Oncology

Department of Oncology, University of Oxford

Old Road Campus Research Building

Off Roosevelt Drive

Oxford OX3 7DQ

Abstract

Background: Patients with pelvic tumours, including bladder, cervix and rectal cancers, receiving radiotherapy are often given additional radiosensitising chemotherapy to improve cure rates, at the expense of increased toxicity. With an ageing population, new approaches to radiosensitisation are urgently required. Inhibition of Histone deacetylase (HDAC) is a promising mechanism of radiosensitisation. Tumour cells may accumulate butyrate which is produced by the gut microbiota via fibre fermentation to sufficient levels to cause HDAC inhibition, due to the Warburg effect. We hypothesised that mice fed a high fibre diet would have improved tumour control following ionising radiation, compared to mice fed a low fibre diet, and that the effects of the diet would be mediated through the gut microbiota.

Results: The faecal (n=59) and caecal (n=59) microbiomes from CD1 nude mice, implanted with RT112 human bladder cancer cell line flank xenografts at the same time as starting low and high fibre (soluble, insoluble, mixed) diets, were similar and they shared the three major taxa (> 80% abundance): *Bacteroidales*, *Clostridales* and *Verrucomicrobiales*. Significantly higher abundance of *Bacteroides acidifaciens* ($p<0.01$) was seen in the gut microbiome of the soluble high fibre (HF) group after 2 weeks of diet. Principal coordinate analysis showed a notable cluster effect within groups, indicating that the diets indeed modified the gut microbiome. Survival analysis by log-rank test showed soluble HF conferred survival benefits, with delayed tumour growth after irradiation (n=32, $p=0.005$). Comparison of the gut microbiomes in the soluble HF group between responders (n=4) and non-responders (n=4) to radiation revealed significantly higher abundance of *B. acidifaciens* in responding mice ($p<0.05$). Predictive metagenomic profiling showed the gut microbiome in responders was enriched for carbohydrate metabolism. To investigate the correlation between specific bacterial taxa and tumour response to radiation, all mice fed with different diets (n=32) were

pooled together, and univariate linear regression revealed a statistically significant positive correlation between the survival time of mice and abundance of *B. acidifaciens* (R^2=0.5278, P<0.001).

Conclusions: High fibre diets sensitised RT112 xenografts to radiation by modifying the gut microbiome and this phenotype was positively correlated with *B. acidifaciens* abundance. These findings might be exploitable for improving radiotherapy response in human patients.

Keywords (up to 10): Gut microbiome, dietary fibre, inulin, cellulose, HDAC inhibition, radiotherapy, radiosensitisation, pelvic tumour, *B.acidifaciens*, *Parabacteroides*

Background

Patients with pelvic tumours, including bladder, cervix and rectal cancers who are receiving radiotherapy are often given additional radiosensitising chemotherapy to improve cure rates, at the expense of increased toxicity in local organs and tissues [1, 2]. With an ageing population, new approaches to radiosensitisation are urgently required. One such approach might be to modify the intake of dietary fibre by supplements before and during radiotherapy or current standard chemoradiation schedules, which would be a very cost-effective strategy, not expected to add to normal tissue toxicity [3, 4].

A high fibre diet has been shown to significantly increase the numbers of short chain fatty acid (SCFA)-producing bacteria in the intestine and faecal levels of SCFA [5], including butyrate, through fermentation of the fibre by the gut microbiota. Butyrate is involved in cellular activities which include mitochondrial activity, G-protein coupled receptors, microbiome homeostasis and histone deacetylase (HDAC) inhibition [6]. Butyrate inhibits HDAC1 and HDAC2 and leads to histone hyperacetylation [7]. Butyrate also stimulates the activity of histone acetyltransferase (HAT) by increasing the essential cofactor acetyl coenzyme A (Acetyl-CoA) [8]. In normal colonocytes, butyrate can act as the primary energy source, which provides about 70% of ATP production, via mitochondrial β-oxidation [9]. However, in cancer cells, decreased use of the Kreb's cycle, along with upregulation of the pentose phosphate pathway and fatty-acid synthesis, results in more butyrate accumulating in the nucleus, to a level sufficient for histone deacetylase inhibition [8].

In mice, high fibre intake has been demonstrated to significantly increase butyrate levels in plasma and tumours [10] and inhibition of HDAC has been proposed as a mechanism of

83 increasing the response of tumour cells to radiation (radiosensitisation). Use of HDAC
84 inhibitors can result in acetylation of histone and non-histone proteins and can inhibit the
85 DNA damage response [11]. We previously found that in mice, the pan-HDAC inhibitor,
86 panobinostat, in combination with ionising radiation (IR) delayed the growth of RT112
87 bladder cancer xenografts but did not worsen local acute (3.75 days) and late (12 weeks)
88 toxicity in the surrounding intestinal tract [12]. The sparing of normal tissue in the gut relative
89 to the tumour is commensurate with the normal gut colonocytes using butyrate as their
90 primary energy source, so butyrate cellular concentrations do not accumulate to levels which
91 can lead to HDAC inhibition.
92
93 As a proof of principle of efficacy of this approach, we tested the hypothesis that mice fed a
94 high fibre diet would have improved tumour control following ionising radiation, compared
95 to mice fed a low fibre diet, and that the effects of the diet would be mediated through the
96 gut microbiota. The aims of this study were: (a) to evaluate the tumour growth in mice treated
97 with high or low fibre diets; (b) to examine the impact of the diet on the microbiome before
98 and after irradiation, and (c) to correlate diet-induced microbiome changes with tumour
99 growth and response to radiation treatment.
100

101 ## Results

102 **The environmental microbiome had minimal impact on gut microbiome analysis and**
103 **dietary fibre content did not affect tumour growth to 50 mm^3**

104 Female CD1 nude mice were injected subcutaneously with RT112 bladder carcinoma cells,
105 and at the same time, they started to receive a modified diet, namely, one of the following:
106 low dietary fibre (0.2% cellulose), low fibre with butyrate in drinking water, high soluble fibre
107 (10% inulin), high insoluble fibre (10% cellulose) and high mixed fibre (5% cellulose, 5% inulin)
108 (Figure 1A and Table S1). By quantification of bacterial loads using PCR and gel electrophoresis,
109 compared to known *E. coli* colony forming unit (CFU) numbers, our mouse samples contained
110 more than 10^4 bacterial CFUs which appeared to override contaminating species in the
111 sample microbial communities (Figure 1B). The PBS negative control was processed
112 identically to the luminal content and tissue samples from the start of the DNA extraction.
113 The nucleic acid amount detected in the PBS negative controls was extremely low, compared
114 to that in the gut microbiota (Figure 1C). Furthermore, the community microbiome in this
115 negative control was very different from the gut microbiome of the mice (Figure 1D).
116 Therefore, the environmental microbiome had minimal impact on the analysis of the gut
117 microbiomes of interest in this study.

118

119 By investigating samples collected when the tumours reached 50 mm^3 and 350 mm^3, the
120 faecal (hereinafter called gut microbiome) and caecal microbiome were found to have similar
121 bacterial components (Figure S1). The mice were culled when their tumours reached 500 mm^3.
122 Butyrate levels in the faeces, validated by high-performance liquid chromatography (HPLC),
123 were generally higher in the low fibre with butyrate and high soluble fibre groups (p=NS;
124 Figure 1E). The mean time for tumours to reach 50 mm^3 was 12.8 ± 1.4 days (Figure 1F).

125

126 **The landscape, diversity and enrichment of bacterial taxa of the gut microbiome in samples**

127 **collected when the tumours reached 50 mm^3**

128 Faeces were collected from culled mice when the tumours reached 50 mm^3. Abundance

129 analysis revealed the five bacterial taxa with the highest abundance were *Bacteroides*

130 *acidifaciens*, *Parabacteroides*, *Akkermansia muciniphila*, *Lachnospiraceae* and *S24-7* (Figure

131 2A). In terms of alpha diversity, the soluble high fibre group had a lower Shannon's index

132 ($p<0.001$) (Figure 2B). This could be due to the higher abundance of *B. acidifaciens,* which

133 lowered the diversity within groups. In terms of beta diversity, principal coordinate analysis

134 showed a notable cluster effect among different groups, which indicates that samples within

135 groups were more similar to each other than to those from the other groups (Figure 2C). This

136 suggested that the gut microbiome was indeed modified in this study, which might be a diet-

137 effect or a cage-effect (see later). Regarding the abundance of specific taxa in different diet

138 groups (Figure 2D), the high soluble fibre diet significantly increased *B. acidifaciens*

139 abundance ($p<0.001$); the low fibre diet increased *Parabacteroides* abundance ($p<0.001$), the

140 low fibre diet with butyrate increased *Akkermansia muciniphila* abundance ($p<0.001$), and

141 the high mixed fibre diet increased *Lachnospiraceae* abundance ($p=0.005$).

142

143 **The landscape, diversity and enrichment of bacterial taxa of the gut microbiome in samples**

144 **collected when the tumours reached 350 mm^3**

145 When the tumours reached 350 mm^3, abundance analysis of the gut microbiome of both IR

146 and non-IR cohorts revealed that the top 6 bacterial taxa with the highest abundance were

147 *S24-7, Akkermansia muciniphila, Bacteroides*, *Lachnospiraceae, Clostridiales* and *B.*

148 *acidifaciens* (Figure 3A). In terms of alpha diversity, the soluble HF group had a significantly

149 lower Shannon's index (p<0.001 for Kruskal-Wallis test) (Figure 3B). In terms of beta diversity,
150 principal coordinate analysis using Bray-Curtis dissimilarity showed a notable clustering effect
151 among different groups, which indicates that samples within groups were more similar to
152 each other than to those from the other groups (Figure 3C). An increased
153 *Firmicutes/Bacteroides* ratio is considered to represent radiation-induced gut dysbiosis [13,
154 14]. Interestingly, only the low fibre group treated with radiation had a trend towards an
155 increased *Firmicutes/Bacteroides* ratio compared to non-irradiated control, but this
156 phenomenon was not seen in the high fibre diet groups, implying that dietary fibre may be
157 protective and therefore reduce gut dysbiosis caused by radiation treatment (Figure S2A).
158 The diets continued to affect the bacterial composition of the gut microbiome as mice got
159 older, up to the time the tumours reached 350 mm^3. The taxonomic cladogram of LEfSe
160 (Linear discriminant analysis Effect size) of the gut microbiome showed that the high soluble
161 fibre diet increased *S24-7* (Figure S2B). Studying the highest abundance bacterial taxa found
162 in the first cohort in this cohort, the relative abundance of *B. acidifaciens*, an acetate-
163 producing bacteria [15, 16], was distributed evenly in different diet groups, except in the
164 soluble HF group with treated with radiation (p=0.200 for Kruskal-Wallis test) (Figure 3D). For
165 the highest abundance bacterial taxa in the second cohort, the relative abundance of
166 *Bacteroidales S24-7* was significantly higher in the mixed HF and soluble HF groups compared
167 to LF and insoluble HF (p=0.001 for Kruskal-Wallis test) (Figure 3E).
168
169 **Soluble high fibre causes increased growth delay in irradiated bladder cancer cell xenografts**
170 **and responses are influenced by the gut microbiota composition.**
171 To investigate the effect of different diets on the tumour response in mice irradiated when
172 the tumour had grown to 50 mm^3, tumour growth was monitored to 350 mm^3. Slopes of the

173 tumour growth curves were obtained using linear regression to indicate the tumour
174 progression rates. The high soluble fibre diet group had the lowest growth rate. The slopes
175 were 4.4 ± 1.3 for LF, 16.1 ± 1.7 for mixed HF, 28.7 ± 1.3 for insoluble HF and 0.4 ± 1.5 for
176 soluble HF (Figure 4A and Figure S3 for individual irradiated mouse tumour growth curves).
177 Kaplan Meier survival curves for time to treble tumour volume showed that the soluble HF
178 group had the longest median survival time (7.5 days for LF, 7 days for mixed HF, 10 days for
179 insoluble HF, 11.5 days for soluble HF; p=0.005, log-rank test) (Figure 4B).
180
181 Among the eight mice fed the soluble high fibre diet, four mice were classified as responders
182 as they had shallower slopes to the tumour growth curves; their slopes were 7.3 ± 1.2, -0.9 ±
183 0.6, -4.8 ± 0.5, -5.2 ± 0.9. The other four mice were classified as non-responders with steeper
184 slopes to the tumour growth curves, namely 34.6 ± 3.0, 31.1 ± 2.6, 23.3 ± 1.0, 33.8 ± 2.9 using
185 linear regression (Figure 4C). In terms of alpha diversity, no significant difference in Shannon's
186 index was shown between responders and non-responders (Figure 4D). In terms of beta
187 diversity, principal coordinate analysis of Bray-Curtis dissimilarity showed the gut microbiome
188 of responders and non-responders were more similar within groups than between groups
189 (Figure 4E).
190
191 **Differences in composition of the gut microbiome between responders and non-responders**
192 Linear discriminant analysis showed that the mice responding to the soluble high fibre diet
193 for a slower tumour growth rate were enriched with *Bacteroidaceae, Flavobacterium,*
194 *Flavobacteriales, Lactococcus, Streptococcus, Streptococcaceae, Allobaculum*,
195 *Erysipelotrichales.* The non-responding tumour-bearing mice were enriched with
196 *Bifidobacterium, Bidifobacteriaceae, Bifidobacteriales, Parabacteroides,*

197 *Porphyromonadaceae, Lactobacillus, Lactobacillaceae* and *Lactobacillales* (Figure 5A). In
198 terms of effect size, *B. acidifaciens* and *Bacteroidaceae* had the largest enrichment in
199 responders, and *Parabacteroides* and *Porphyromonadaceae* had the largest enrichment in
200 non-responders (Figure 5B). To further explore these findings, the discrete false-discovery
201 rates within all taxonomic levels were calculated (Figure 5C). In responders, *B. acidifaciens*
202 species and the *Allobaculum* genus and in non-responders *Lactobacillus* and *Parabacteroides*
203 had p-values <0.05, highlighting the significance of these findings. The *B.acidifaciens*
204 abundance was significantly higher in responders than that in non-responders (p=0.29)
205 (Figure 5D), while the *Bacteroidales S24-7* abundance was similar between responders and
206 non-responders in the soluble HF group (p=0.200) (Figure 5E).
207
208 **Correlation between the abundance of *B. acidifaciens* or *Parabacteroides* genus and mouse**
209 **survival time in IR and non-IR cohorts**
210 As *B. acidifaciens* was the 'top hit' for responders in the soluble HF group, we explored how
211 specific bacterial taxa affected mouse survival time. The correlation between *B. acidifaciens*
212 abundance and time to culling was investigated across the diet groups. Some mice in the non-
213 IR cohort lived as long as those in the IR cohort, ie. >40 days, which may be a reflection of 6
214 Gy being a relatively low dose of radiation (Figure S4A). In the IR cohort, the time of culling
215 positively correlated with *B. acidifaciens* abundance (R^2=0.528, p<0.001). However, a similar
216 correlation was not seen in the non-IR cohort (R^2=0.085, p=0.357). Using the time for tumours
217 to treble in volume as the outcome measure, mice with high *B. acidifaciens* abundance had a
218 significantly prolonged median survival time (Log-rank test: p<0.001) (Figure 6A). A similar
219 finding was seen in the IR cohort (p=0.003), but not in the non-IR cohort (p=0.236). To further
220 identify specific unfavourable bacterial taxa which might offset the effect of radiation, the

221 *Parabacteroides* genus, was selected, as one of the top two 'hits' for non-responders in the
222 soluble HF group. This was investigated for the association between its abundance and time
223 to culling (Figure S4B). In the IR cohort, the time to culling negatively correlated with the
224 abundance of *Parabacteroides* genus (Figure S4B; R^2=0.164, p=0.022). However, a similar
225 correlation was not seen in the non-IR cohort (R^2=0.084, p=0.360). Using the time for tumours
226 to treble in volume as the outcome measure, mice in the low *Parabacteroides* genus
227 abundance group had no significant difference in median survival time compared to the high
228 abundance group (Log-rank test: p=0.374) (Figure 6B). *B. acidifaciens* (p=0.200 for Kruskal-
229 Wallis test) and *Parabacteroides* genus (p=0.005 for Kruskal-Wallis test) abundance was
230 evenly distributed among all cages, which suggested that the existence of this taxa in the gut
231 microbiome was not a cage-specific effect (Figure S5 and Table S2).
232
233 **Metagenomics functional prediction of the gut microbiome by response in the soluble HF**
234 **group**
235 Functional prediction at KEGG (Kyoto Encyclopedia of Genes and Genomes) pathways level 2
236 revealed that the gut microbiome in responders was enriched for carbohydrate metabolism
237 pathways and in non-responders for membrane transport pathways (Figure 7A). To further
238 explore this at KEGG pathways level 3, enrichment of the amino sugar and nucleotide sugar
239 metabolism pathway was shown in responders with enrichment of the ATP-binding cassette
240 (ABC) transporter pathway shown in non-responders (Figure 7B).
241

242 ## Discussion

243 In 2016, Wei et al. demonstrated that up to four-fold-higher levels of butyrate accumulated
244 in the lymphoma flank xenograft tumours of mice fed a high fibre diet compared to a low
245 fibre diet [10]. Butyrate has been proposed to increase histone deacetylase inhibition, which
246 is a known mechanism of cellular radiosensitisation [8, 11]. Therefore, the gut microbiota in
247 mice fed a high fibre diet might act as an endogenous radiosensitiser, by providing a
248 sufficiently high systemic butyrate level.

249

250 In this study, faecal and caecal microbiomes were investigated in mice fed with low fibre diets,
251 low fibre diets with butyrate, high mixed fibre diets, high insoluble fibre diets and high soluble
252 fibre diets, and profiles of both microbiomes were correlated with each other. The gut
253 microbiomes were shaped in mice fed with different modified diets for two weeks and
254 homogeneous gut microbiomes were seen in samples within groups. A distinct bacterial taxon
255 was seen in each group: enrichment of *B. acidifaciens* in soluble HF, *Parabacteroides* in LF,
256 *Akkermansia muciniphila* in LF with butyrate, and *Lachnospiraceae* in mixed HF. To date, there
257 is only limited literature studying the effects of dietary fibre intake or the gut microbiota on
258 tumour growth. Hardman et al. suggested that breast cancer xenografts grew more slowly in
259 mice fed with fish oil concentrate than those tumours of control mice [17]. In contrast,
260 Cougnoux et al. proposed that Colibactin-producing *E. coli* enhanced tumour growth of colon
261 cancer xenografts [18]. In our study, no significant difference for the time for tumours to
262 reach 50 mm^3 was seen in mice from different groups. This demonstrated that diet and the
263 diet-modified microbiome had no effect on tumour growth, up to that point.

264

265 The tumours were irradiated when they reached a volume of 50 mm^3 and monitored until
266 they reached 350 mm^3. As the mice aged during the time required for tumour growth, all mice
267 were enriched for the S24-7 family. This indicated that their gut microbiomes had altered over
268 the tumour growth period. Although the gut microbiomes became more heterogeneous, a
269 notable cluster effect still existed in samples within groups. Mice responding to radiation in
270 the soluble HF group were enriched with *B. acidifaciens* and non-responding mice were
271 enriched with the *Parabacteroides* genus. A predictive metagenomics study of the gut
272 microbiome in responders was enriched with carbohydrate metabolism pathways. This
273 suggested that fermentation of carbohydrate, possibly soluble fibre, was enriched in
274 responders and its final products, namely, butyrate and/or other short-chain fatty acids,
275 might contribute to the radiosensitisation. When the mice from different diet groups were
276 pooled, *B. acidifaciens* abundance was positively correlated with survival time and mice with
277 high *B. acidifaciens* had the longest median survival times using Kaplan-Meier survival analysis.
278
279 Early studies have shown that dietary fibre, such as wheat bran, can be protective against
280 colonic adenomas. Since then, systemic reviews have also provided some evidence that
281 dietary fibre intake is inversely associated with the risk of breast cancer [19], pancreatic
282 cancer [20], prostate cancer [21] and ovarian cancer [22]. Most of the early studies are limited
283 to epidemiology studies. Other healthy lifestyle factors, such as exercise, abstention from
284 smoking and alcohol, etc., rather than high fibre intake, could be major confounding biases in
285 these studies.
286
287 More recently it has emerged that one of the major mechanisms by which dietary fibre intake
288 protects against cancer is the modulation of the gut microbiota [23], via short chain fatty acid

289 production and immunomodulation. Dysbiosis has been linked to colorectal cancer, and a
290 recent study proposed stage-distinct alterations in the tumourigenesis of colorectal cancer
291 [24]; *Atopobium parvulum* and *Actinomyces odontolyticus* were significantly enriched in
292 multiple polypoid adenomas and intramucosal carcinomas, and *Fusobacterium nucleatum*
293 increased continuously from the intramucosal carcinoma to more advanced stages.
294 *Helicobacter pylori* is the most famous and early-defined link between a bacterium and cancer
295 [25]. Nowadays, *H. pylori* eradication has become one of the most promising treatments in
296 the prevention of gastric cancer [26].
297
298 In this study, in CD1 nude mice, short-term high fibre intake alone and its modifying influence
299 on the gut microbiota had no effect on tumour progression rate (to 50 mm^3). Gopalakrishnan
300 et al. demonstrated that the gut microbiota can enhance melanoma responses to anti-PD-L1,
301 possibly via enhanced systemic and anti-tumour immunity [27]. Sivan et al. suggested that
302 commensal *Bifidobacterium* are associated with enhanced anti-PD-L1 efficacy, via increased
303 cytotoxic T cell accumulation in the tumour microenvironment [28]. Furthermore, the
304 immune-stimulatory effect of CTLA-4 blockage was found to be dependent on *B.*
305 *thetaiotaomicron* or *B. fragilis* [29].
306
307 All of these recent studies proposed that a modified gut microbiota can augment the efficacy
308 of anti-tumoural treatment. However, most of them are limited to chemotherapy and
309 immunotherapy [30]. To date, this is the first study to suggest that a high soluble fibre diet,
310 with the related modified gut microbiome, can act as a radiosensitiser. Innate immunity plays
311 a role in shaping the gut microbiota and adaptive immunity has a strong impact on tumour
312 progression or treatment response. Our studies were conducted in immunodeficient CD-1

313 nude mice, which implies that the radiosensitising effect of dietary fibre here was
314 independent of immunomodulation. This does not rule out the tantalising possibility that this
315 radiosensitisation could be further enhanced by immunomodulatory effects in an
316 immunocompetent environment. This is worthy of further investigation.
317
318 *B. acidifaciens* abundance was enhanced by a high soluble fibre diet in this study and *B.*
319 *acidifaciens* was identified as a potential radiosensitiser because its abundance was positively
320 correlated with tumour response to radiation and survival time in the IR cohort. This
321 bacterium was first isolated in 2000 and was so named because its reduces the pH level of
322 peptone-yeast broth with Fildes' digest [16]. Consistent with our findings, Marques et al.
323 demonstrated that a high-fibre diet markedly increased the prevalence of *B acidifaciens* [31].
324 Another previous study also showed *B. acidifaciens* to be enriched in normal human controls,
325 compared to patients with inflammatory bowel disease [32]. Yang et al. found that *B.*
326 *acidifaciens* increased insulin sensitivity and further prevented obesity [33]. However, the
327 effect of this bacteria on tumour growth is still controversial. A study showed that increasing
328 *B. acidifaciens* abundance was seen in hepatocellular carcinoma which was induced by a
329 streptozotocin-high fat diet [34]. However, *B. acidifaciens* reduces isoflavones, a chemical
330 that is associated with increased risk of breast cancer [35]. *B. acidifaciens* was also shown to
331 contribute to the anti-tumour effect of medicinal Gynostemma saponins [36].
332 In terms of the immune context, IL-6 and IL-10 have been found to be augmented by *B.*
333 *acidifaciens* via enhancement of MHC class II molecules expression and also co-stimulatory
334 molecules (i.e., CD80 and CD86) on antigen presenting cells [37]. *B. acidifaciens* has also been
335 shown to promote IgA antibody production in the large intestine [38, 39], with a protective

336 effect on the mucosa of large intestine, which could be exploited to reduce normal tissue
337 toxicity of irradiation.
338
339 We also found *Bacteroidales S24-7* (or *Candidatus Homeothermaceae* [40] or *Muribaculaceae*
340 [41]), an uncultured bacterium with limited information, to be highly abundant in our study,
341 especially in the mixed HF and soluble HF group. The prevalence of this bacterium in humans
342 is 20% [42]. An increased prevalence of Bacteroidales S24-7 of up to 70% was shown in the
343 Hadza tribe of Tanzania who consume tubers containing large amounts of soluble fibre [42].
344
345 Colonic inulin fermentation in healthy humans produces much higher levels of acetate than
346 that of propionate and butyrate [43]. Also, *Bacteroidetes,* including *B. acidifaciens*, have been
347 proposed to produce the end products acetate, succinate and possibly propionate, but not
348 butyrate [15, 16]. Acetate levels in plasma are 3 fold higher than that of propionate and
349 butyrate [44], and acetate production is enhanced in tumours due to hyperactive metabolism
350 occuring during the Warburg effect [45]. It is also worth noting that synthesis of acetyl-coA
351 from acetate is a critical substrate to enhance histone acetylation levels by histone
352 acetyltransferase (HAT) [45], and HDAC inhibition by acetate has been shown in several
353 previous studies [46, 47]. These findings suggest that acetate might initiate an alternative
354 mechanism of radiosensitisation other than via butyrate.
355
356 Integrating these findings, the mouse responders in the soluble HF group had a higher
357 abundance of acetate-producing bacteria (*B. acidifaciens*) which might be able to ferment
358 inulin to provide higher acetate levels which could then act as a substrate for butyrate
359 production, given that acetate is necessary for butyrate production particularly in the butyryl-

360 CoA:acetate CoA-transferase pathway [48, 49]. We speculate that the butyrate levels could
361 be enhanced due to cross-feeding of butyrate-producing bacteria by *Bacteroides acidifaciens*.
362 Interestingly, Ramirez-Farias et al. have showed that inulin increased both acetate-producing
363 bacteria (*Faecalibacterium prausnitzii*) and butyrate-producing bacteria (*Bifidobacterium*
364 *adolescentis*) in their human volunteer study [50]. Proof-of-concept has been demonstrated
365 by cross-feeding *Faecalibacterium prausnitzii* and *Bifidobacterium adolescentis* which
366 enhances butyrate formation [51]. In our study, most plasma butyrate levels (with one sample
367 showing 98 µM) and all tumour butyrate levels could not be resolved above the signal to noise
368 of the chromatogram (limit of quantification 10 µM) but this does not rule out that the effect
369 comes from butyrate.
370
371 We have highlighted several possible mechanisms underlying the radiosensitising effects of
372 high soluble fibre diets or *B. acidifaciens,* which need further investigation in future studies:
373 (1) increased concentrations of butyrate or other short-chain fatty acids in tumours, which
374 can act by HDAC inhibition or via other mechanisms; (2) suppression of overgrowth of
375 unfavourable bacteria, e.g. possibly inhibiting *Parabacteroides* genus; and/or (3)
376 enhancement of anti-tumoural immunity. In this study, two findings, namely, (1) the positive
377 correlation between the time of culling and *B. acidifaciens* abundance and (2) the dose-
378 dependent effect of *B. acidifaciens* abundance on time for tumours to treble in volume
379 supported the hypothesis that the action of a high fibre diet on the gut microbiota may induce
380 radiosensitisation in mouse xenograft tumours.
381
382 Environmental contamination is an inevitable issue in microbiome studies [52]. To minimise
383 the influence of contamination in this study, bacterial loads of samples were quantified and

384 appropriate negative controls were included. Bacterial loads from luminal content and tissue
385 samples contained more than 10^4 CFUs which overrode the environmental bacteria
386 communities. Furthermore, the bacterial compositions of the PBS negative controls were very
387 different from those of the study groups, so the environmental microbiome was considered
388 not to be a major source of bias in this study.
389
390 Although a strong correlation between *B. acidifaciens* abundance and tumour response to
391 irradiation was seen, further studies are needed to validate a causal relationship between *B.*
392 *acidifaciens* and radiosensitisation of bladder and other pelvic tumours.
393

394 **Conclusions**

395 A high soluble fibre diet increased responses of RT112 mouse xenografts to irradiation and
396 this phenotype was associated with higher relative abundance of *B. acidifaciens*. Human
397 patients may respond to dietary fibre supplementation before and during radiotherapy to
398 achieve tumour radiosensitisation via modification of the gut microbiome.
399

400 # Methods

401 **Overview of study design**

402 In this study, we aimed to evaluate the tumour growth after irradiation in mice fed high or
403 low fibre diets and to correlate diet-induced microbiome changes with tumour growth. Two
404 cohorts of CD1 nude female mice were studied. Two types of samples were collected, namely
405 faeces and caecal contents. The samples from the first cohort were collected when the
406 tumours had grown to 50 mm^3, and consisted of 15 mice in five groups (n=3 per group) fed
407 diets comprising: low fibre (< 0.2% cellulose), low fibre with butyrate (98% sodium butyrate,
408 Sigma Aldrich), high mixed fibre (5% cellulose, 5% inulin), high insoluble fibre (10% cellulose),
409 high soluble fibre (10% inulin) (see Table S1 for details). These diets were formulated by Jia-
410 Yu Ke at Research Diets, Inc. on 11/6/2018. The samples from the second cohort were
411 collected when the tumours had reached 350 mm^3 either without (n=3) or following (n=8)
412 radiation, and consisted of four groups fed diets comprising: low fibre, high soluble fibre, high
413 insoluble fibre and high mixed fibre. 16S rRNA gene sequencing was performed on a MiSeq
414 platform to investigate the bacterial components of the mouse gut microbiome.
415 Metagenomic analysis was conducted using a QIIME2 platform to identify the features
416 (differentially abundant taxa or diversity index) that correlated to the phenotype.

417 **Mice and mouse diets**

418 CD1-nude female mice (Charles River Laboratories, USA 6-7 weeks) were housed in a
419 temperature-controlled environment with a 12-h reversed-phase light/dark cycle (lights on
420 21:00 h) and provided with food and water *ad libitum*. At 7 to 8 weeks of age, mice were
421 injected subcutaneously with RT112 bladder cancer cells (DSMZ, Germany) and started
422 receiving either a low fibre diet (2 g cellulose/3850 kcal), a high insoluble fibre diet (100 g
423 cellulose/3850 kcal), a high soluble fibre diet (100 g inulin/3850 kcal) or a high mixed fibre

424 diet (50 g cellulose + 50 g inulin / 3850 kcal) for a maximum time of 9 weeks or until they were
425 culled when the tumours reached 350 mm^3. Faeces, caecal contents, and proximal and distal
426 colons from the first cohort were taken when the tumour reached 50 mm^3 (each group n=3)
427 without irradiation to investigate the microbiome at baseline. Faeces and caecal contents
428 from the second cohort were taken when the tumour reached 350 mm^3 after IR (each group
429 n=8) or without IR (each group n=3) or at the end of study (9 weeks after xenograft) to study
430 the association between the gut microbiome composition and tumour response.

431 **Xenograft model and irradiation method**

432 Mice were injected subcutaneously under anaesthesia into the right flank with 5 x 10^6 human
433 bladder cancer cells (RT112) in RPMI medium (Sigma Aldrich) with phenol red-free Matrigel
434 (BD Biosciences) at a total volume of 100 μl (1:1 ratio cell suspension to Matrigel). Tumour
435 growth was measured three times a week and size determined by calipers using (length x
436 width x height x π/6). To assess the effects of different dietary fibres on tumour growth after
437 irradiation *in vivo*, mice received ionising radiation to the tumour (6 Gy, single fraction, 300
438 kV, using a Gulmay-320 cabinet irradiator, Xstrahl Inc, UK). A dose of 6 Gy was chosen due to
439 the promising effect in our previous radiosensitisation experiments with a HDAC inhibitor
440 (manuscript in preparation.)

441 **Microbiome sample collection and DNA extraction**

442 All samples were transported on ice and kept at -20°C for less than 2 hours before DNA
443 extraction. Bacterial genomic DNA was extracted using a DNeasy PowerSoil DNA Isolation Kit
444 (QIAGEN Ltd, Manchester, UK), as per the Human Microbiome Project [53]. Briefly, by adding
445 sodium dodecyl sulfate (SDS), microbial cells were lysed by mechanical disruption with a
446 ceramic bead set on 3,000 rpm for 10 minutes, followed by binding of DNA tightly to a silica
447 membrane in a Spin Filter device at high salt concentrations. Eventually, DNA was collected

448 into sterile elution buffer and quantified using a NanoDrop spectrophotometer. All DNA
449 samples were kept at -80°C. All samples were collected and handled in sterile containers and
450 equipment to minimise contamination. Those sent for sequencing (Omega
451 Bioservices,Georgia, USA) were dried in an Eppendorf concentrator 5301 (Eppendorf North
452 America Inc, USA) at a rotational speed of 1,400 rpm and centrifugal force of 240 x g for 1
453 hour at 30°C.

454 **Faecal butyrate levels quantification**

455 Faecal samples were first homogenised in ice cold Millipore Synergy purified water.
456 Thereafter, 20 µL of sample or standard was taken and 10 µL of internal standard (valeric acid,
457 Alfa Aesar, UK) added prior to the addition of 5 µL 15% percholoric acid. Samples were mixed
458 and centrifuged at 12,000 g for 15 min at 4°C followed by direct injection (10 µL) of the
459 supernatant. High-performance liquid chromatography (HPLC) separation was carried out
460 using a Waters Acquity H-Class Quarternary Solvent Manager with mobile phases of 0.1%
461 formic acid in water (A) and methanol (B) and a gradient of 35-75% B on a Waters Acquity
462 CSH C18, 1.7 µm, 100 x 2.1 column. Butyrate and internal standard (IS) were detected by mass
463 spectrometry with a Waters Acquity TQ detector in positive electrospray ionisation mode.
464 Butyrate was detected with a cone voltage of 20 V at selected ion recording (SIR) of *m/z* 88.41
465 (M+H) and IS with a cone voltage of 15 V and SIR of *m/z* 103.2 (M+H).

466 **Identification and quantification of bacterial DNA**

467 The microbiota of the contents of the intestinal tracts and the intestinal wall of the proximal
468 and distal colon (tissue) was quantified by PCR of 16S rRNA. This was performed on genomic
469 DNA extracted as described above. The PCR was performed using primers - V3F
470 (CCAGACTCCTACGGGAGGCAG) and V3R (CGTATTACCGCGGCTGCTG) [54]. All primers were
471 purchased from Sigma. For each sample, Phire Tissue Direct PCR Master Mix (Thermo Fisher

472 Scientific) was used to amplify the 16S rRNA gene hypervariable V3 region (product size = 200
473 bp). PCR amplifications were performed using the following conditions: 98°C for 5 minutes
474 followed by 35 cycles at 98°C for 5 seconds each, 66.3°C for 5 seconds, and 72°C for
475 30 seconds and a final extension step at 72°C for 1 minute. The amplification products were
476 visualised on a 1% agarose gel after electrophoretic migration of 5 µl of amplified material. A
477 standard curve was created from serial dilutions of *Escherichia Coli* from 1 x 10^2, 1 x 10^4, 1
478 x10^6 colony-forming units (CFU) which was quantified by CFU assay. All samples were run in
479 duplicate. In CFU assay, 20 µL of serial dilution of *E. Coli* was incubated onto Luria-Bertani (LB)
480 agar plates, and colonies were counted and bacterial concentrations of the original samples
481 were estimated after 24 hours incubation.

482 **Bacterial 16S rRNA gene sequencing**

483 16S rRNA gene sequencing methods were adapted from the methods developed for the NIH-
484 Human Microbiome Project [53, 55]. The amplification and sequencing of 16S rRNA gene
485 V3V4 region were done commercially by Omega Bioservices (Georgia, USA) on a MiSeq
486 platform (Illumina, Inc, San Diego, CA) using the 2x300 bp paired-end protocol, yielding
487 paired-end reads with near-complete overlap. The primers containing adapters for Miseq
488 sequencing were used for amplification and single-end barcodes, allowing pooling and direct
489 sequencing of PCR products [56]. PBS negative controls were included to eliminate the
490 confounding effects of environmental contamination.

491 All 16S rRNA gene-based metagenomic analysis was conducted using a QIIME2 platform [57].
492 Quality filtered sequences with >97% identity were clustered into bins known as Operational
493 Taxonomic Units (OTUs), using open-reference OTU picking. The relative abundance of each
494 OTU was obtained from all samples. In the taxonomic analysis, the microbiome at the phylum,

495 class, order, family, genus and species levels was classified with reference to the Greengenes
496 database [58].
497 The analysis pipeline was as follows:
498 i. All sequences were trimmed to a length of 240, since the quality dropped above
499 this length based on the sequence quality plots.
500 ii. De-noised sequencing errors by using the "Deblur" plugin in QIIME2 [59].
501 iii. Taxonomic assignment was performed with Greengenes [60] by the "feature-
502 classifier" command.
503 iv. To visualise the differences in microbial composition between gut contents and
504 tissue, a taxonomic profile was generated by conducting differential abundance
505 analysis using balances in gneiss.
506 v. To identify the features characterising the differences between groups, the LEfSe
507 method of analysis was performed to compare abundances of all bacterial clades
508 [61]. By validation using the Kruskal-Wallis test at the α setting of 0.05, effect size
509 was obtained by LDA (linear discriminant analysis) based on the significantly
510 different vectors resulting from the comparison of abundances between groups.
511 vi. To validate the significance of enrichment of bacterial taxa among different
512 groups, discrete false-discovery rates (DS-FDR) were calculated [62]
513 vii. A phylogenetic tree was generated by using the "phylogeny" plugin in QIIME2.
514 viii. To investigate the alpha and beta diversity, the diversity commands of "alpha-
515 group-significance" and "beta-group-significance" were used to obtain Shannon's
516 index, and Bray-Curtis dissimilarity. A principal coordinates (PCoA) plot was
517 obtained by using the Emperor Tool based on the results of Bray-Curtis
518 dissimilarities.

519 ix. The OTU table was rarefied using the “alpha-rarefraction” command in QIIME2.
520 The alpha rarefraction plot showed the richness of the samples with increasing
521 sequence count.
522 x. To predict the metagenome functional profiles, PICRUSt, a bioinformatics
523 software package, was used to collapse predicted functions (KEGG Orthology; KO)
524 based on 16S rRNA surveys into higher categories (KEGG pathway) after picking
525 OTUs and normalisation [63].

526 **Statistical analysis**

527 Power calculations for the number of mice per group were done using G*Power software
528 version 3.1.9.4 [64]. Alpha diversity and relative abundance of specific bacterial taxa were
529 compared using the Kruskal-Wallis test following by Dunn’s multiple comparison test. All mice
530 were classified into high, intermediate or low diversity groups based on tertiles of distribution.
531 Time to treble in volume was defined as the interval (in days) from the date of irradiation
532 (growth to 50 mm^3) to the date for the tumour to treble in volume. Tumour growth curves
533 were analysed for each group, and their slopes were compared using one-way ANOVA. The
534 LEfSe method of analysis was applied to determine the difference in bacterial taxa, using the
535 Kruskal-Wallis test. Significantly different taxa presented from the previous comparison
536 applying LEfSe method were used as input for LDA, which produced an LDA score. Volcano
537 plots showed the significance of the taxa which are different among different groups, with
538 log_{10} (FDR-adjusted p-values) on the y-axis and median-adjusted effect sizes on the x-axis. In
539 addition, mice were also classified as having high, intermediate and low abundance of *B.*
540 *acidifaciens* or high and low abundance of *parabacteroides* genus based on the relative
541 abundance of these taxa in the gut microbiome sample. All analyses were conducted in
542 QIIME2 and GraphPad Prism version 8.0 (La Jolla, CA).

543 **List of abbreviations**

ABC	ATP-binding cassette
B. acidifaciens	*Bacteroides acidifaciens*
BBN	N-butyl-N-(4-hydroxybutyl)-nitrosamine
CFU	colony formation unit
E. Coli	Escherichia coli
FDA	false-discovery rate
Gy	Gray
HAT	histone acetyltransferase
HDAC	histone deacetylase
HF	high fibre
Insoluble HF	insoluble high fibre
IR	irradiation
KEGG	Kyoto Encyclopedia of Genes and Genomes
LC-MS	liquid chromatography–mass spectrometry
LDA	linear discriminant analysis
LEFSe	linear discriminant analysis effect size
LF	low fibre
LF+B	low fibre plus butyrate
MIBC	muscle-invasive bladder cancer
Mixed HF	mixed high fibre
OTU	operational taxonomic unit
PCoA	principal coordinates analysis
PICRUSt	Phylogenetic Investigation of Communities by Reconstruction of Unobserved States
SCFA	short chain fatty acid
SDS	sodium dodecyl sulfate
Soluble HF	soluble high fibre

544

545 ## Declarations

546 **Ethics approval and consent to participate**

547 All animal procedures were performed in accordance with the ARRIVE guidelines. All animal
548 protocols were approved by the University of Oxford Clinical Medicine Animal Welfare Ethics
549 Review Board and conducted under animal project licenses (PPL) P4B738A3B and P8484EDAE

550 **Consent for publication**

551 Not applicable

552 **Availability of data and material**

553 Raw 16S rRNA reads and metadata have been made available in Figshare
554 (https://figshare.com/projects/The_gut_microbiota_may_drive_the_radiosensitising_effect
555 _of_a_high_fibre_diet/68393).

556 **Competing interests**

557 The authors declare that they have no competing interests.

558 **Funding**

559 This work was funded by Cancer Research UK Programme grant C5255/A23755. The funding
560 body had no role in the design of the study, collection, analysis, interpretation of data or in
561 writing the manuscript.

562 **Author's contributions**

563 CKT extracted the DNA from mouse samples, performed the analysis and interpretation of
564 the data and drafted the manuscript. SP performed the animal experiments, collected the
565 faeces, caecal contents, intestinal tissue and blood. AH measured the faecal butyrate levels.
566 AEK conceived the study, supervised the work, and revised the manuscript. All authors read
567 and approved the final manuscript.

568 **Acknowledgements**

569 We thank Professor Simon Kroll and Dr Anderson Ryan for their very helpful comments. We
570 thank Dr Jia-Yu Ke at Research Diets, Inc. for formulation of the mouse diets, Dr Lisa Folkes
571 for assistance with the faecal butyrate quantification and Omega Bioservices (Georgia, USA)
572 for the 16S rRNA gene sequencing on a MiSeq platform.

573 **References**

574 1. Viswanathan AN, Lee LJ, Eswara JR, Horowitz NS, Konstantinopoulos PA, Mirabeau-
575 Beale KL, et al. Complications of pelvic radiation in patients treated for gynecologic
576 malignancies. Cancer 2014;(24):3870-3883.
577 2. Nishimura Y. Rationale for chemoradiotherapy. Int J Clin Oncol 2004;(6):414-420.
578 3. Wedlake L, Shaw C, McNair H, Lalji A, Mohammed K, Klopper T, et al. Randomized
579 controlled trial of dietary fiber for the prevention of radiation-induced
580 gastrointestinal toxicity during pelvic radiotherapy. Am J Clin Nutr 2017;(3):849-857.
581 4. Hedelin M, Skokic V, Wilderang U, Ahlin R, Bull C, Sjoberg F, et al. Intake of citrus
582 fruits and vegetables and the intensity of defecation urgency syndrome among
583 gynecological cancer survivors. PLoS One 2019;(1):e0208115.
584 5. Bishehsari F, Engen PA, Preite NZ, Tuncil YE, Naqib A, Shaikh M, et al. Dietary Fiber
585 Treatment Corrects the Composition of Gut Microbiota, Promotes SCFA Production,
586 and Suppresses Colon Carcinogenesis. Genes-Basel 2018;(2).
587 6. Bourassa MW, Alim I, Bultman SJ, Ratan RR. Butyrate, neuroepigenetics and the gut
588 microbiome: Can a high fiber diet improve brain health? Neurosci Lett 2016;(56-63.
589 7. Davie JR. Inhibition of histone deacetylase activity by butyrate. J Nutr 2003;(7
590 Suppl):2485S-2493S.
591 8. Donohoe DR, Collins LB, Wali A, Bigler R, Sun W, Bultman SJ. The Warburg effect
592 dictates the mechanism of butyrate-mediated histone acetylation and cell
593 proliferation. Mol Cell 2012;(4):612-626.
594 9. Roediger WE. Role of anaerobic bacteria in the metabolic welfare of the colonic
595 mucosa in man. Gut 1980;(9):793-798.
596 10. Wei W, Sun W, Yu S, Yang Y, Ai L. Butyrate production from high-fiber diet protects
597 against lymphoma tumor. Leuk Lymphoma 2016;(10):2401-2408.
598 11. Groselj B, Sharma NL, Hamdy FC, Kerr M, Kiltie AE. Histone deacetylase inhibitors as
599 radiosensitisers: effects on DNA damage signalling and repair. Br J Cancer
600 2013;(4):748-754.
601 12. Groselj B, Ruan JL, Scott H, Gorrill J, Nicholson J, Kelly J, et al. Radiosensitization In
602 Vivo by Histone Deacetylase Inhibition with No Increase in Early Normal Tissue
603 Radiation Toxicity. Mol Cancer Ther 2018;(2):381-392.
604 13. Lavrinienko A, Mappes T, Tukalenko E, Mousseau TA, Moller AP, Knight R, et al.
605 Environmental radiation alters the gut microbiome of the bank vole Myodes
606 glareolus. Isme J 2018;(11):2801-2806.
607 14. Wang AP, Ling ZX, Yang ZX, Kiela PR, Wang T, Wang C, et al. Gut Microbial Dysbiosis
608 May Predict Diarrhea and Fatigue in Patients Undergoing Pelvic Cancer
609 Radiotherapy: A Pilot Study. Plos One 2015;(5).
610 15. Macy JM, Probst I. The biology of gastrointestinal bacteroides. Annu Rev Microbiol
611 1979;(561-594.
612 16. Miyamoto Y, Itoh K. Bacteroides acidifaciens sp. nov., isolated from the caecum of
613 mice. Int J Syst Evol Microbiol 2000;(145-148.
614 17. Hardman WE, Munoz J, Jr., Cameron IL. Role of lipid peroxidation and antioxidant
615 enzymes in omega 3 fatty acids induced suppression of breast cancer xenograft
616 growth in mice. Cancer Cell Int 2002;(1):10.

617 18. Cougnoux A, Dalmasso G, Martinez R, Buc E, Delmas J, Gibold L, et al. Bacterial
618 genotoxin colibactin promotes colon tumour growth by inducing a senescence-
619 associated secretory phenotype. Gut 2014;(12):1932-1942.
620 19. Aune D, Chan DS, Greenwood DC, Vieira AR, Rosenblatt DA, Vieira R, et al. Dietary
621 fiber and breast cancer risk: a systematic review and meta-analysis of prospective
622 studies. Ann Oncol 2012;(6):1394-1402.
623 20. Wang CH, Qiao C, Wang RC, Zhou WP. Dietary fiber intake and pancreatic cancer
624 risk: a meta-analysis of epidemiologic studies. Sci Rep 2015;(10834.
625 21. Deschasaux M, Pouchieu C, His M, Hercberg S, Latino-Martel P, Touvier M. Dietary
626 total and insoluble fiber intakes are inversely associated with prostate cancer risk. J
627 Nutr 2014;(4):504-510.
628 22. Huang X, Wang X, Shang J, Lin Y, Yang Y, Song Y, et al. Association between dietary
629 fiber intake and risk of ovarian cancer: a meta-analysis of observational studies. J Int
630 Med Res 2018;(10):3995-4005.
631 23. Zeng H, Lazarova DL, Bordonaro M. Mechanisms linking dietary fiber, gut microbiota
632 and colon cancer prevention. World J Gastrointest Oncol 2014;(2):41-51.
633 24. Yachida S, Mizutani S, Shiroma H, Shiba S, Nakajima T, Sakamoto T, et al.
634 Metagenomic and metabolomic analyses reveal distinct stage-specific phenotypes of
635 the gut microbiota in colorectal cancer. Nat Med 2019;(6):968-976.
636 25. Uemura N, Okamoto S, Yamamoto S, Matsumura N, Yamaguchi S, Yamakido M, et al.
637 Helicobacter pylori infection and the development of gastric cancer. N Engl J Med
638 2001;(11):784-789.
639 26. Suzuki H, Matsuzaki J. Gastric cancer: evidence boosts Helicobacter pylori
640 eradication. Nat Rev Gastroenterol Hepatol 2018;(8):458-460.
641 27. Gopalakrishnan V, Spencer CN, Nezi L, Reuben A, Andrews MC, Karpinets TV, et al.
642 Gut microbiome modulates response to anti-PD-1 immunotherapy in melanoma
643 patients. Science 2018;(6371):97-103.
644 28. Sivan A, Corrales L, Hubert N, Williams JB, Aquino-Michaels K, Earley ZM, et al.
645 Commensal Bifidobacterium promotes antitumor immunity and facilitates anti-PD-L1
646 efficacy. Science 2015;(6264):1084-1089.
647 29. Vetizou M, Pitt JM, Daillere R, Lepage P, Waldschmitt N, Flament C, et al. Anticancer
648 immunotherapy by CTLA-4 blockade relies on the gut microbiota. Science
649 2015;(6264):1079-1084.
650 30. Alexander JL, Wilson ID, Teare J, Marchesi JR, Nicholson JK, Kinross JM. Gut
651 microbiota modulation of chemotherapy efficacy and toxicity. Nat Rev Gastroenterol
652 Hepatol 2017;(6):356-365.
653 31. Marques FZ, Nelson E, Chu PY, Horlock D, Fiedler A, Ziemann M, et al. High-Fiber Diet
654 and Acetate Supplementation Change the Gut Microbiota and Prevent the
655 Development of Hypertension and Heart Failure in Hypertensive Mice. Circulation
656 2017;(10):964-977.
657 32. Ott SJ, Musfeldt M, Wenderoth DF, Hampe J, Brant O, Folsch UR, et al. Reduction in
658 diversity of the colonic mucosa associated bacterial microflora in patients with active
659 inflammatory bowel disease. Gut 2004;(5):685-693.
660 33. Yang JY, Lee YS, Kim Y, Lee SH, Ryu S, Fukuda S, et al. Gut commensal Bacteroides
661 acidifaciens prevents obesity and improves insulin sensitivity in mice. Mucosal
662 Immunol 2017;(1):104-116.

663 34. Xie G, Wang X, Liu P, Wei R, Chen W, Rajani C, et al. Distinctly altered gut microbiota
664 in the progression of liver disease. Oncotarget 2016;(15):19355-19366.
665 35. Renouf M, Hendrich S. Bacteroides uniformis is a putative bacterial species
666 associated with the degradation of the isoflavone genistein in human feces. J Nutr
667 2011;(6):1120-1126.
668 36. Chen L, Tai WC, Brar MS, Leung FC, Hsiao WL. Tumor grafting induces changes of gut
669 microbiota in athymic nude mice in the presence and absence of medicinal
670 Gynostemma saponins. PLoS One 2015;(5):e0126807.
671 37. Tsuda M, Hosono A, Yanagibashi T, Hachimura S, Hirayama K, Itoh K, et al. Prior
672 stimulation of antigen-presenting cells with Lactobacillus regulates excessive
673 antigen-specific cytokine responses in vitro when compared with Bacteroides.
674 Cytotechnology 2007;(2-3):89-101.
675 38. Yanagibashi T, Hosono A, Oyama A, Tsuda M, Hachimura S, Takahashi Y, et al.
676 Bacteroides induce higher IgA production than Lactobacillus by increasing activation-
677 induced cytidine deaminase expression in B cells in murine Peyer's patches. Biosci
678 Biotechnol Biochem 2009;(2):372-377.
679 39. Yanagibashi T, Hosono A, Oyama A, Tsuda M, Suzuki A, Hachimura S, et al. IgA
680 production in the large intestine is modulated by a different mechanism than in the
681 small intestine: Bacteroides acidifaciens promotes IgA production in the large
682 intestine by inducing germinal center formation and increasing the number of IgA+ B
683 cells. Immunobiology 2013;(4):645-651.
684 40. Ormerod KL, Wood DLA, Lachner N, Gellatly SL, Daly JN, Parsons JD, et al. Genomic
685 characterization of the uncultured Bacteroidales family S24-7 inhabiting the guts of
686 homeothermic animals. Microbiome 2016;(
687 41. Lagkouvardos I, Lesker TR, Hitch TCA, Galvez EJC, Smit N, Neuhaus K, et al. Sequence
688 and cultivation study of Muribaculaceae reveals novel species, host preference, and
689 functional potential of this yet undescribed family. Microbiome 2019;(1):28.
690 42. Ormerod KL, Wood DL, Lachner N, Gellatly SL, Daly JN, Parsons JD, et al. Genomic
691 characterization of the uncultured Bacteroidales family S24-7 inhabiting the guts of
692 homeothermic animals. Microbiome 2016;(1):36.
693 43. Boets E, Deroover L, Houben E, Vermeulen K, Gomand SV, Delcour JA, et al.
694 Quantification of in Vivo Colonic Short Chain Fatty Acid Production from Inulin.
695 Nutrients 2015;(11):8916-8929.
696 44. Louis P, Hold GL, Flint HJ. The gut microbiota, bacterial metabolites and colorectal
697 cancer. Nat Rev Microbiol 2014;(10):661-672.
698 45. Bose S, Ramesh V, Locasale JW. Acetate Metabolism in Physiology, Cancer, and
699 Beyond. Trends Cell Biol 2019;(9):695-703.
700 46. Soliman ML, Rosenberger TA. Acetate supplementation increases brain histone
701 acetylation and inhibits histone deacetylase activity and expression. Mol Cell
702 Biochem 2011;(1-2):173-180.
703 47. Bolduc JF, Hany L, Barat C, Ouellet M, Tremblay MJ. Epigenetic Metabolite Acetate
704 Inhibits Class I/II Histone Deacetylases, Promotes Histone Acetylation, and Increases
705 HIV-1 Integration in CD4(+) T Cells. J Virol 2017;(16).
706 48. Vital M, Howe AC, Tiedje JM. Revealing the bacterial butyrate synthesis pathways by
707 analyzing (meta)genomic data. MBio 2014;(2):e00889.
708 49. Vital M, Karch A, Pieper DH. Colonic Butyrate-Producing Communities in Humans: an
709 Overview Using Omics Data. mSystems 2017;(6).

710 50. Ramirez-Farias C, Slezak K, Fuller Z, Duncan A, Holtrop G, Louis P. Effect of inulin on
711 the human gut microbiota: stimulation of Bifidobacterium adolescentis and
712 Faecalibacterium prausnitzii. Brit J Nutr 2009;(4):541-550.
713 51. Rios-Covian D, Gueimonde M, Duncan SH, Flint HJ, de los Reyes-Gavilan CG.
714 Enhanced butyrate formation by cross-feeding between Faecalibacterium prausnitzii
715 and Bifidobacterium adolescentis. Fems Microbiol Lett 2015;(21).
716 52. Eisenhofer R, Minich JJ, Marotz C, Cooper A, Knight R, Weyrich LS. Contamination in
717 Low Microbial Biomass Microbiome Studies: Issues and Recommendations. Trends
718 Microbiol 2019;(2):105-117.
719 53. Human Microbiome Project C. A framework for human microbiome research. Nature
720 2012;(7402):215-221.
721 54. Wang HY, Du PC, Li J, Zhang YY, Zhang W, Han N, et al. Comparative analysis of
722 microbiome between accurately identified 16S rDNA and quantified bacteria in
723 simulated samples. J Med Microbiol 2014;(433-440.
724 55. Human Microbiome Project C. Structure, function and diversity of the healthy
725 human microbiome. Nature 2012;(7402):207-214.
726 56. Caporaso JG, Lauber CL, Walters WA, Berg-Lyons D, Huntley J, Fierer N, et al. Ultra-
727 high-throughput microbial community analysis on the Illumina HiSeq and MiSeq
728 platforms. ISME J 2012;(8):1621-1624.
729 57. Hall M, Beiko RG. 16S rRNA Gene Analysis with QIIME2. Methods Mol Biol
730 2018;(113-129.
731 58. Balvociute M, Huson DH. SILVA, RDP, Greengenes, NCBI and OTT - how do these
732 taxonomies compare? Bmc Genomics 2017;(
733 59. Nearing JT, Douglas GM, Comeau AM, Langille MGI. Denoising the Denoisers: an
734 independent evaluation of microbiome sequence error-correction approaches. Peerj
735 2018;(
736 60. DeSantis TZ, Hugenholtz P, Larsen N, Rojas M, Brodie EL, Keller K, et al. Greengenes,
737 a chimera-checked 16S rRNA gene database and workbench compatible with ARB.
738 Appl Environ Microb 2006;(7):5069-5072.
739 61. Segata N, Izard J, Waldron L, Gevers D, Miropolsky L, Garrett WS, et al. Metagenomic
740 biomarker discovery and explanation. Genome Biology 2011;(6).
741 62. Jiang L, Amir A, Morton JT, Heller R, Arias-Castro E, Knight R. Discrete False-Discovery
742 Rate Improves Identification of Differentially Abundant Microbes. mSystems
743 2017;(6).
744 63. Langille MG, Zaneveld J, Caporaso JG, McDonald D, Knights D, Reyes JA, et al.
745 Predictive functional profiling of microbial communities using 16S rRNA marker gene
746 sequences. Nat Biotechnol 2013;(9):814-821.
747 64. Faul F, Erdfelder E, Lang AG, Buchner A. G*Power 3: A flexible statistical power
748 analysis program for the social, behavioral, and biomedical sciences. Behav Res
749 Methods 2007;(2):175-191.
750

751

752 ## Figure legends

753 **Figure 1. The environmental microbiome had minimal impact on gut microbiome analysis**
754 **and dietary fibre content did not affect tumour growth to 50 mm^3**

755 (A) Two microbiomes were analysed from the intestinal tract, namely, faecal and caecal
756 content samples collected when tumours reached 50 mm^3 and 350 mm^3 respectively. (B)
757 Quantification of bacterial load from different tissue and luminal contents from mice, with *E.*
758 *Coli* (1×10^2, 1×10^4, 1×10^6 CFUs) as controls (n=1 mouse). (C) Comparison of the total amount
759 of nucleic acid quantified by PicoGreen assay in all samples collected when the tumours
760 reached 50 mm^3 and 350 mm^3. (D) Common bacterial taxa at the species level in 4 samples
761 of PBS, as negative controls of DNA extraction by 16S rRNA sequencing. (E) Butyrate level in
762 the faeces at the time of culling, which was between 11-16 days. (F) All mice were culled when
763 tumours had reached 50 mm^3, between 11 to 16 days after tumour inoculation, average 12.8
764 (STD $\pm$ 1.4) days.

765 **Figure 2. Dietary fibre shapes the baseline gut microbiome when tumours reached 50 mm^3**.
766 (A) Stacked bar plot of phylogenetic composition of common bacterial taxa at the species
767 level when tumours reached 50 mm^3. Faeces were collected from mice fed with low fibre, low
768 fibre with butyrate, high mixed fibre, high insoluble fibre and high soluble fibre diets (n=3 for
769 each group). (B) Shannon's index of gut microbiomes by Kruskal-Wallis test. Error bars
770 represent the interquartile range of diversity scores. (C) Principal coordinate analysis of gut
771 microbiomes using Bray-Curtis dissimilarity. A notable clustering effect by diet was seen in
772 the gut microbiome. (D) Differentially abundant taxa when the tumours reached 50 mm^3. All
773 comparisons among different diet groups was performed by Kruskal-Wallis test and Dunn's
774 multiple comparison tests. All tests compared each median with the 'control' denoted. The
775 diet with the highest abundance of a taxa was denoted as the control. *P<0.05; **P<0.01.

776 **Figure 3. Composition of the gut microbiome when tumours reached 350 mm^3**. (A) Stacked
777 bar plot of the phylogenetic composition of common bacterial taxa at the species level when
778 tumours reached 350 mm^3. Samples were collected from mice fed with low fibre, high mixed
779 fibre, high insoluble fibre and high soluble fibre diets (n=8 for each group). (B) Shannon's
780 index of gut microbiomes by Kruskal-Wallis test. Error bars represent the interquartile range
781 of diversity scores. (C) Principal coordinate analysis of gut microbiomes using Bray-Curtis
782 dissimilarity. Relative abundance of (D) *B. acidifaciens* and (E) *Bacteroidales S24-7* in mice
783 with or without irradiation.

784 **Figure 4. Soluble high fibre causes increased growth delay in irradiated bladder cancer cell**
785 **xenografts and responses are influenced by the gut microbiota composition.** (A) Tumour
786 growth in RT112 flank xenografts irradiated with 6 Gy IR, in mice fed low fibre, high mixed
787 fibre, high insoluble fibre and high soluble fibre diets (n=8 for each group). Slopes of tumour
788 curves were calculated by linear regression to represent tumour growth rates and compared
789 by ANOVA. (B) Kaplan–Meier survival curves for mice with RT112 xenografts showing plots of
790 time to treble tumour volume. (C) Mice were stratified into responders and non-responders
791 based on the tumour response to radiation. (D) Shannon's index of gut microbiota in
792 responders and non-responders by Kruskal-Wallis test. Error bars represent the interquartile
793 range of diversity scores. (E) Principal coordinate analysis of gut samples (n=8) in soluble HF
794 group by response using Bray-Curtis dissimilarity.

795 **Figure 5. Differences in composition of the gut microbiome between responders and non-**
796 **responders.** (A) Taxonomic cladogram from LEfSe showing differences of taxa in responders
797 and non-responders of soluble HF group. Dot size is proportional to the abundance of the
798 taxon. (B) Linear discriminant analysis (LDA) scores computed for differentially abundant taxa
799 in the microbiomes of responders (green) and non-responders (red). Length indicates the

800 effect size associated with a taxon, p=0.05, Kruskal-Wallis test. (C) Discrete false-discovery
801 rate of different abundant taxa in responders and non-responders in the soluble HF group.
802 Differential abundance within all taxonomic levels in responders versus non-responders by
803 Mann-Whitney U test. Dots are overlapping between *Bacteroides acidifaciens* and
804 *Allobaculum*, and between *Lactobacillus* and *Parabacteroides*. Relative abundance of (D) *B.*
805 *acidifaciens* and (E) *Bacteroidales S24-7* and in responders and non-responders in the soluble
806 HF group.

807 **Figure 6. Abundance of OTUs within the gut microbiome is predictive of response to ionising**
808 **irradiation.** Kaplan-Meier (KM) plots of time for tumours to treble in volume, whole cohorts,
809 IR cohorts, non-IR cohorts, based on (A) *B. acidifaciens* or (B) *Parabacteroides* genus
810 abundance in IR and Non-IR cohorts from different diet groups combined. Comparison KM
811 plots by log-rank test in mice with high abundance (green; relative abundance > 0.1),
812 intermediate abundance (red; 0.1 > relative abundance > 0.01), or low abundance (blue; 0.01
813 > relative abundance) of *B. acidifaciens* in all, IR and non-IR cohorts. For *Parabacteroides*
814 genus, relative abundance more than or equal to 0.01 was classified as high (blue), while less
815 than 0.01 was classified as low (green).

816 **Figure 7. A favourable gut microbiome is associated with enhanced carbohydrate**
817 **metabolism.** Metagenomic functional prediction by PICRUSt of the gut microbiome in
818 responders (n=4) and non-responders (n=4) in the soluble HF group with reference to the
819 KEGG database (A) level 2 and (B) level 3. Columns represent mice (responders, orange; non-
820 responders, blue), and rows represent enrichment of predicted KEGG pathways (red, low
821 enrichment; yellow, medium enrichment; blue, high enrichment).

822

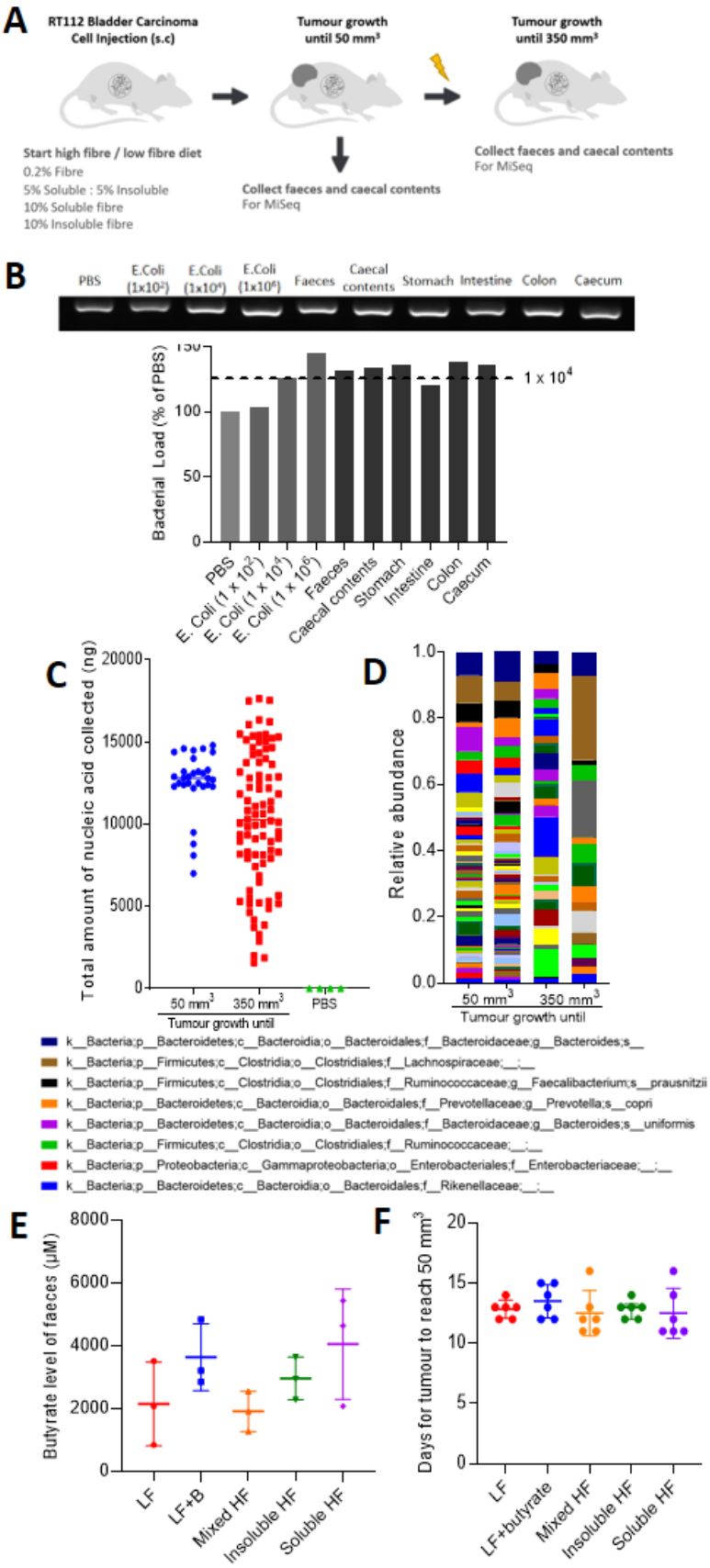
A
RT112 Bladder Carcinoma Cell Injection (s.c)
Tumour growth until 50 mm³
Tumour growth until 350 mm³
Start high fibre / low fibre diet
0.2% Fibre
5% Soluble : 5% Insoluble
10% Soluble fibre
10% Insoluble fibre
Collect faeces and caecal contents
For MiSeq
Collect faeces and caecal contents
For MiSeq
B
PBS
E.Coli (1x10²)
E.Coli (1x10⁴)
E.Coli (1x10⁶)
Faeces
Caecal contents
Stomach
Intestine
Colon
Caecum
Bacterial Load (% of PBS)
1 x 10⁴
C
Total amount of nucleic acid collected (ng)
50 mm³
350 mm³
PBS
Tumour growth until
D
Relative abundance
50 mm³
350 mm³
Tumour growth until
k__Bacteria;p__Bacteroidetes;c__Bacteroidia;o__Bacteroidales;f__Bacteroidaceae;g__Bacteroides;s__
k__Bacteria;p__Firmicutes;c__Clostridia;o__Clostridiales;f__Lachnospiraceae;__;__
k__Bacteria;p__Firmicutes;c__Clostridia;o__Clostridiales;f__Ruminococcaceae;g__Faecalibacterium;s__prausnitzii
k__Bacteria;p__Bacteroidetes;c__Bacteroidia;o__Bacteroidales;f__Prevotellaceae;g__Prevotella;s__copri
k__Bacteria;p__Bacteroidetes;c__Bacteroidia;o__Bacteroidales;f__Bacteroidaceae;g__Bacteroides;s__uniformis
k__Bacteria;p__Firmicutes;c__Clostridia;o__Clostridiales;f__Ruminococcaceae;__;__
k__Bacteria;p__Proteobacteria;c__Gammaproteobacteria;o__Enterobacteriales;f__Enterobacteriaceae;__;__
k__Bacteria;p__Bacteroidetes;c__Bacteroidia;o__Bacteroidales;f__Rikenellaceae;__;__
E
Butyrate level of faeces (µM)
LF
LF+B
Mixed HF
Insoluble HF
Soluble HF
F
Days for tumour to reach 50 mm³
LF
LF+butyrate
Mixed HF
Insoluble HF
Soluble HF

Figure 1

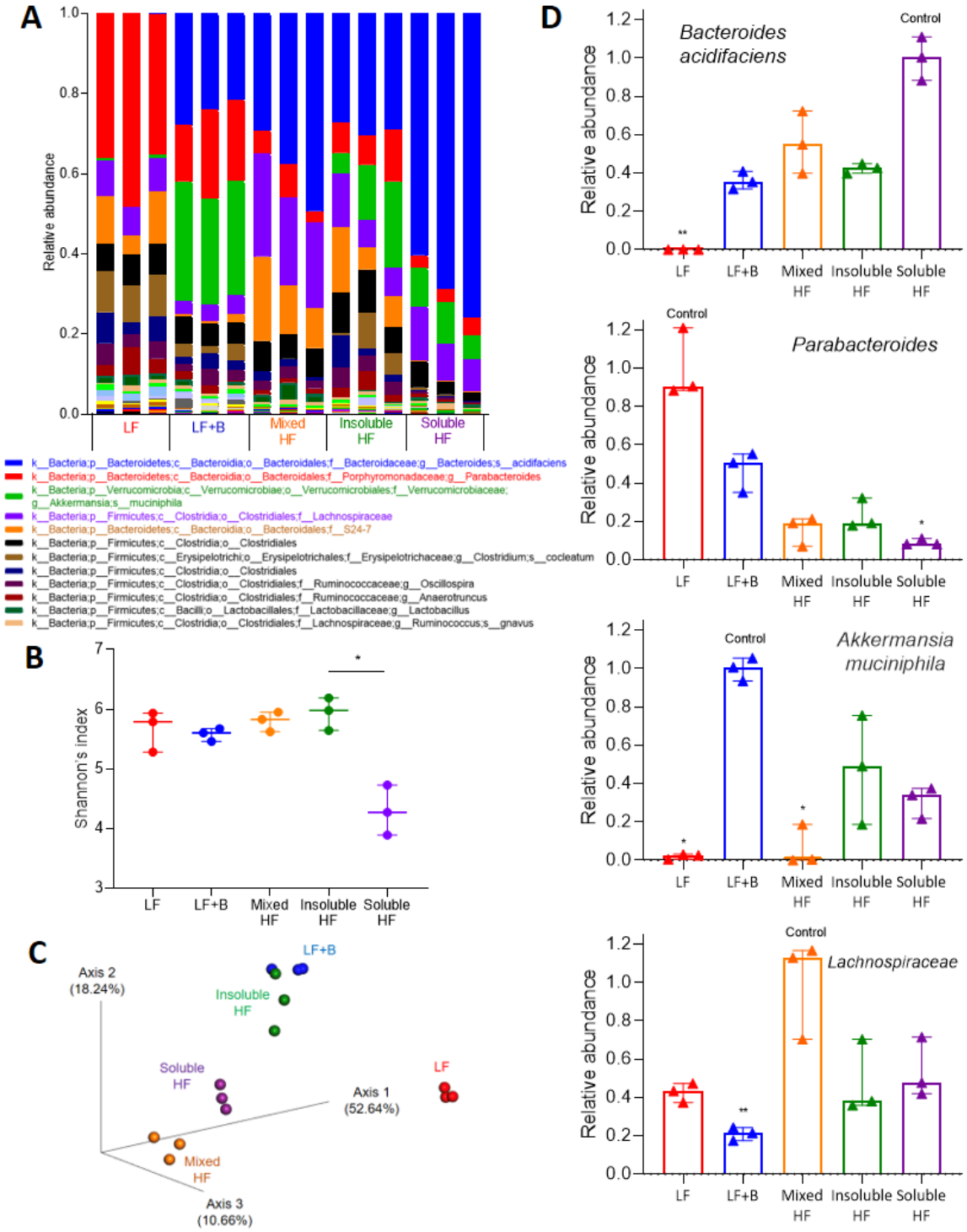
A
Relative abundance
LF
LF+B
Mixed HF
Insoluble HF
Soluble HF
k__Bacteria;p__Bacteroidetes;c__Bacteroidia;o__Bacteroidales;f__Bacteroidaceae;g__Bacteroides;s__acidifaciens
k__Bacteria;p__Bacteroidetes;c__Bacteroidia;o__Bacteroidales;f__Porphyromonadaceae;g__Parabacteroides
k__Bacteria;p__Verrucomicrobia;c__Verrucomicrobiae;o__Verrucomicrobiales;f__Verrucomicrobiaceae;g__Akkermansia;s__muciniphila
k__Bacteria;p__Firmicutes;c__Clostridia;o__Clostridiales;f__Lachnospiraceae
k__Bacteria;p__Bacteroidetes;c__Bacteroidia;o__Bacteroidales;f__S24-7
k__Bacteria;p__Firmicutes;c__Clostridia;o__Clostridiales
k__Bacteria;p__Firmicutes;c__Erysipelotrichi;o__Erysipelotrichales;f__Erysipelotrichaceae;g__Clostridium;s__cocleatum
k__Bacteria;p__Firmicutes;c__Clostridia;o__Clostridiales
k__Bacteria;p__Firmicutes;c__Clostridia;o__Clostridiales;f__Ruminococcaceae;g__Oscillospira
k__Bacteria;p__Firmicutes;c__Clostridia;o__Clostridiales;f__Ruminococcaceae;g__Anaerotruncus
k__Bacteria;p__Firmicutes;c__Bacilli;o__Lactobacillales;f__Lactobacillaceae;g__Lactobacillus
k__Bacteria;p__Firmicutes;c__Clostridia;o__Clostridiales;f__Lachnospiraceae;g__Ruminococcus;s__gnavus
B
Shannon's index
C
Axis 2 (18.24%)
Axis 1 (52.64%)
Axis 3 (10.66%)
D
Bacteroides acidifaciens
Parabacteroides
Akkermansia muciniphila
Lachnospiraceae
Control

Figure 2

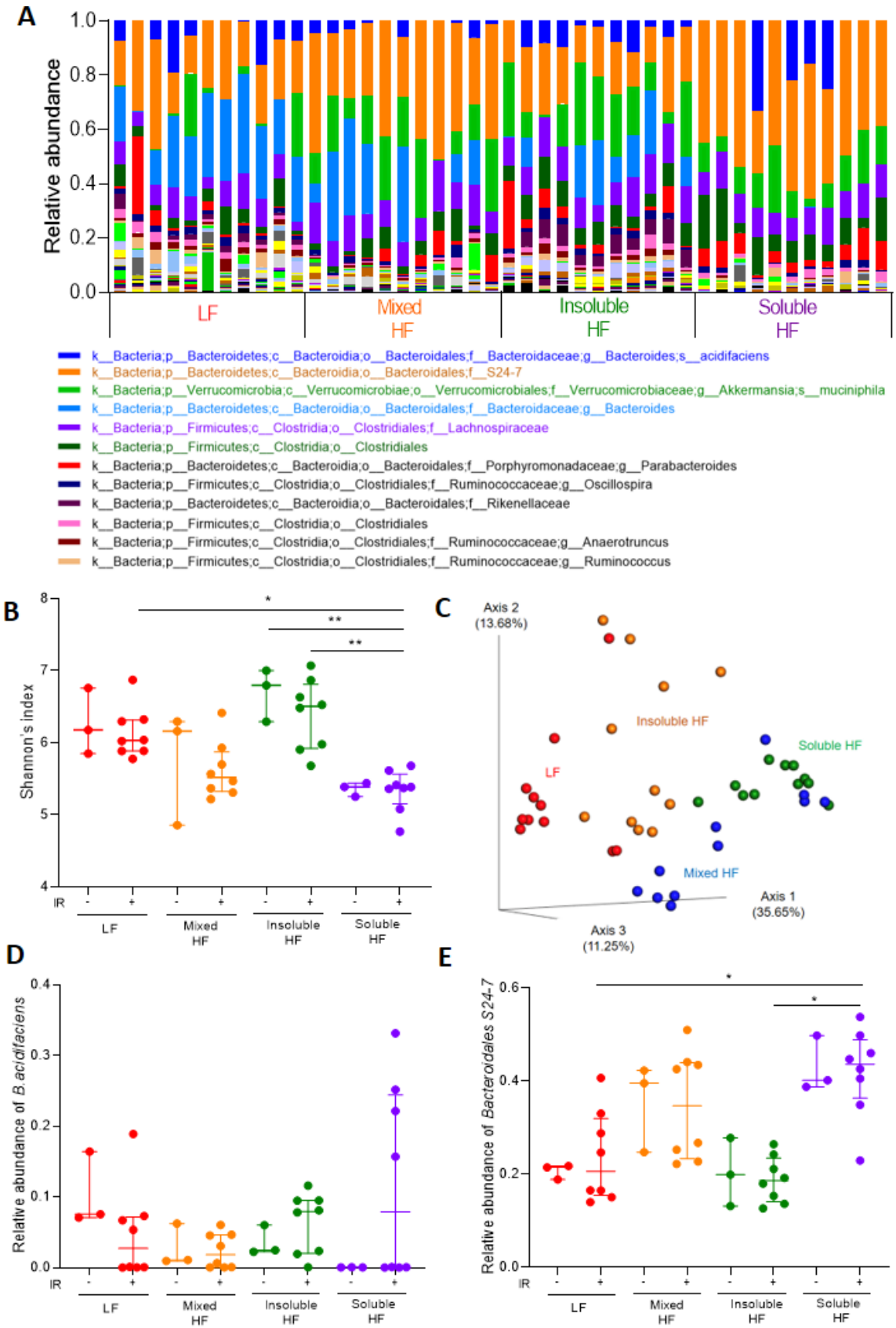
A
Relative abundance
1.0
0.8
0.6
0.4
0.2
0.0
LF
Mixed HF
Insoluble HF
Soluble HF
k__Bacteria;p__Bacteroidetes;c__Bacteroidia;o__Bacteroidales;f__Bacteroidaceae;g__Bacteroides;s__acidifaciens
k__Bacteria;p__Bacteroidetes;c__Bacteroidia;o__Bacteroidales;f__S24-7
k__Bacteria;p__Verrucomicrobia;c__Verrucomicrobiae;o__Verrucomicrobiales;f__Verrucomicrobiaceae;g__Akkermansia;s__muciniphila
k__Bacteria;p__Bacteroidetes;c__Bacteroidia;o__Bacteroidales;f__Bacteroidaceae;g__Bacteroides
k__Bacteria;p__Firmicutes;c__Clostridia;o__Clostridiales;f__Lachnospiraceae
k__Bacteria;p__Firmicutes;c__Clostridia;o__Clostridiales
k__Bacteria;p__Bacteroidetes;c__Bacteroidia;o__Bacteroidales;f__Porphyromonadaceae;g__Parabacteroides
k__Bacteria;p__Firmicutes;c__Clostridia;o__Clostridiales;f__Ruminococcaceae;g__Oscillospira
k__Bacteria;p__Bacteroidetes;c__Bacteroidia;o__Bacteroidales;f__Rikenellaceae
k__Bacteria;p__Firmicutes;c__Clostridia;o__Clostridiales
k__Bacteria;p__Firmicutes;c__Clostridia;o__Clostridiales;f__Ruminococcaceae;g__Anaerotruncus
k__Bacteria;p__Firmicutes;c__Clostridia;o__Clostridiales;f__Ruminococcaceae;g__Ruminococcus
B
Shannon's index
8
7
6
5
4
*
**
**
IR
-
+
LF
Mixed HF
Insoluble HF
Soluble HF
C
Axis 2 (13.68%)
Insoluble HF
Soluble HF
LF
Mixed HF
Axis 1 (35.65%)
Axis 3 (11.25%)
D
Relative abundance of B.acidifaciens
0.4
0.3
0.2
0.1
0.0
E
Relative abundance of Bacteroidales S24-7
0.6
0.4
0.2
0.0
*
*

Figure 3

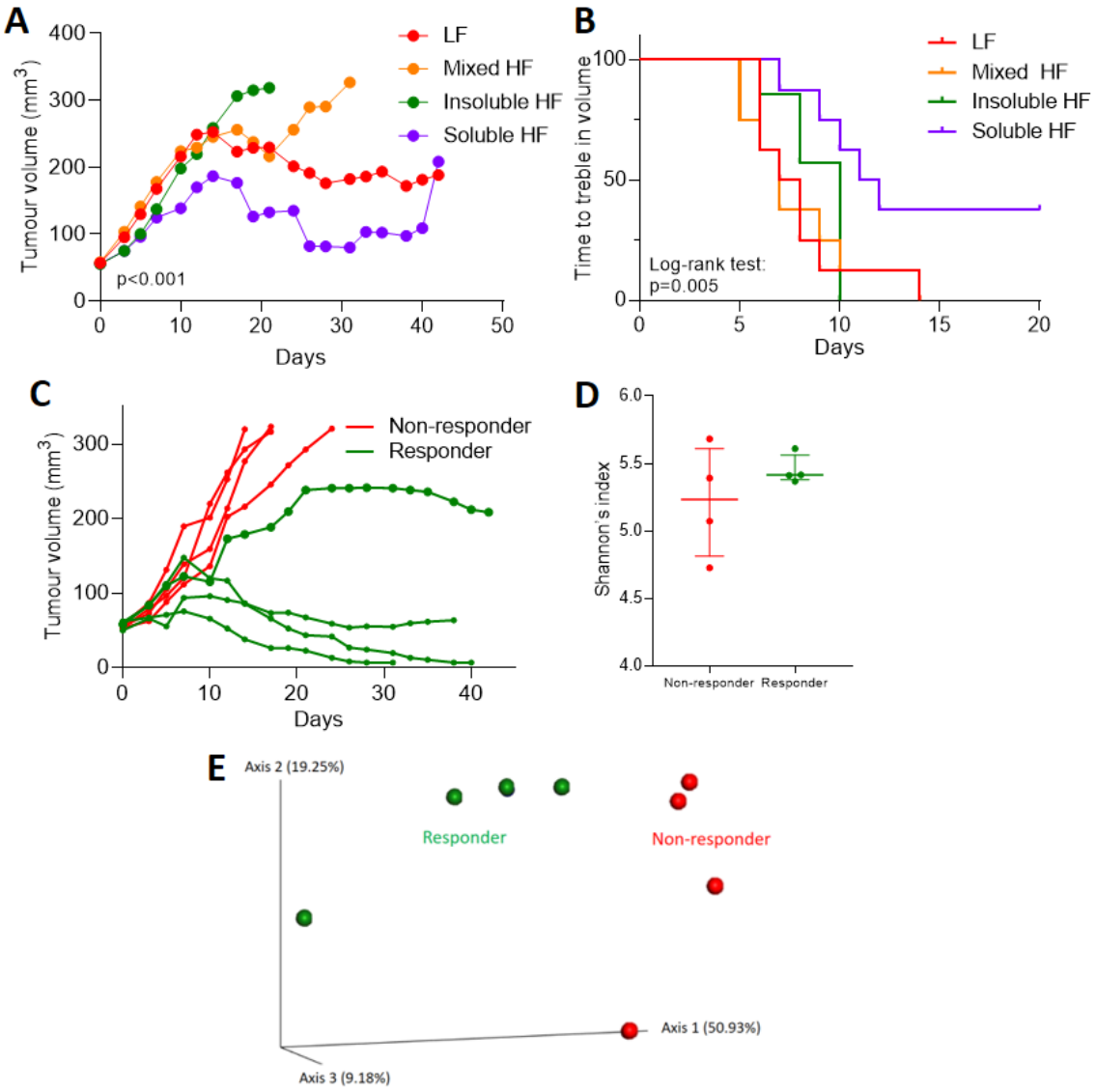
A
Tumour volume (mm3)
400
300
200
100
0
0
10
20
30
40
50
Days
p<0.001
LF
Mixed HF
Insoluble HF
Soluble HF
B
Time to treble in volume
100
50
0
0
5
10
15
20
Days
Log-rank test:
p=0.005
LF
Mixed HF
Insoluble HF
Soluble HF
C
Tumour volume (mm3)
300
200
100
0
0
10
20
30
40
Days
Non-responder
Responder
D
Shannon's index
6.0
5.5
5.0
4.5
4.0
Non-responder
Responder
E
Axis 2 (19.25%)
Responder
Non-responder
Axis 1 (50.93%)
Axis 3 (9.18%)

Figure 4

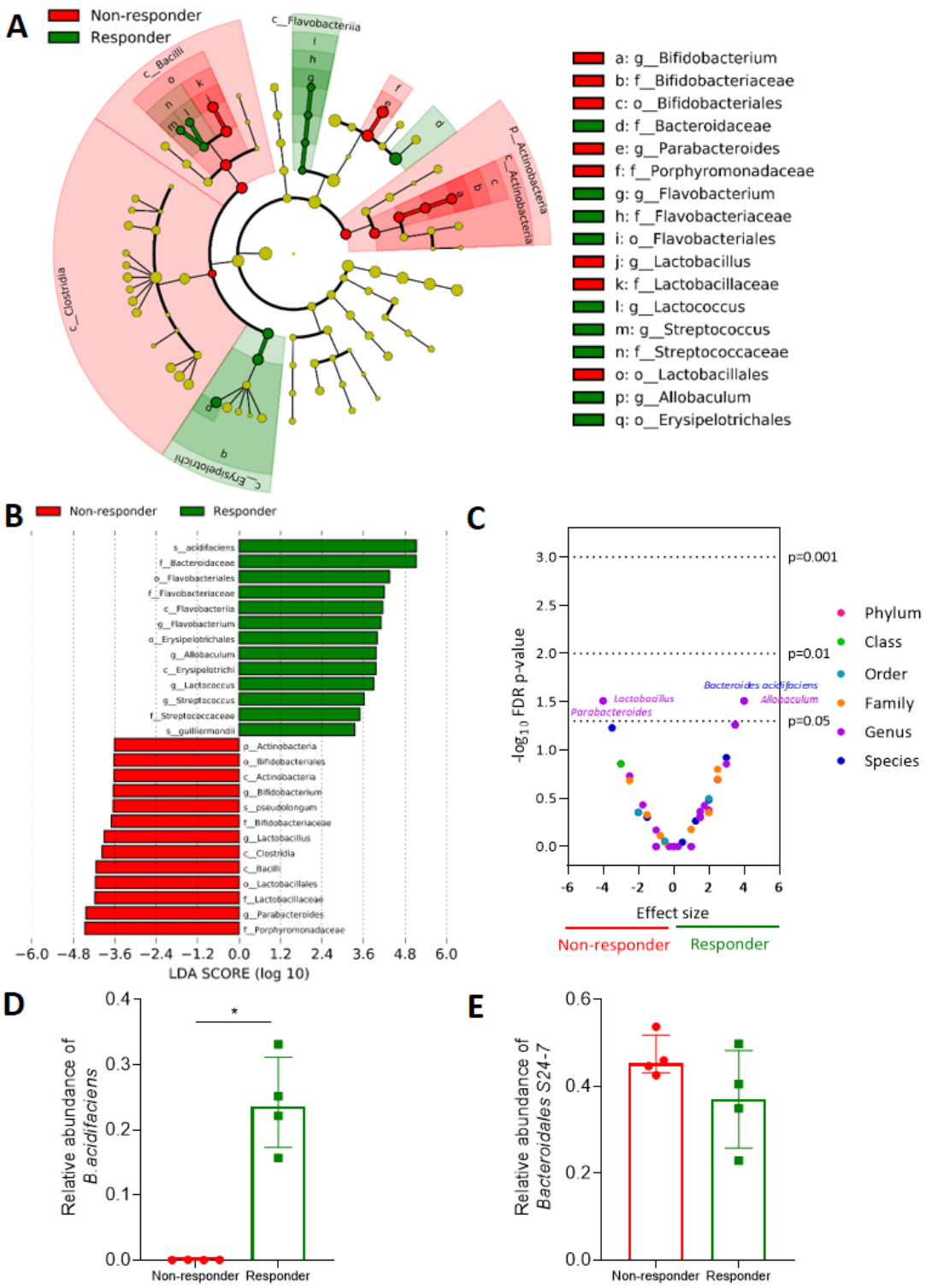
A
Non-responder
Responder
c__Flavobacteriia
c__Bacilli
p__Actinobacteria
c__Actinobacteria
c__Clostridia
c__Erysipelotrichi
a: g__Bifidobacterium
b: f__Bifidobacteriaceae
c: o__Bifidobacteriales
d: f__Bacteroidaceae
e: g__Parabacteroides
f: f__Porphyromonadaceae
g: g__Flavobacterium
h: f__Flavobacteriaceae
i: o__Flavobacteriales
j: g__Lactobacillus
k: f__Lactobacillaceae
l: g__Lactococcus
m: g__Streptococcus
n: f__Streptococcaceae
o: o__Lactobacillales
p: g__Allobaculum
q: o__Erysipelotrichales
B
Non-responder
Responder
s__acidifaciens
f__Bacteroidaceae
o__Flavobacteriales
f__Flavobacteriaceae
c__Flavobacteriia
g__Flavobacterium
o__Erysipelotrichales
g__Allobaculum
c__Erysipelotrichi
g__Lactococcus
g__Streptococcus
f__Streptococcaceae
s__guilliermondii
p__Actinobacteria
o__Bifidobacteriales
c__Actinobacteria
g__Bifidobacterium
s__pseudolongum
f__Bifidobacteriaceae
g__Lactobacillus
c__Clostridia
c__Bacilli
o__Lactobacillales
f__Lactobacillaceae
g__Parabacteroides
f__Porphyromonadaceae
−6.0 −4.8 −3.6 −2.4 −1.2 0.0 1.2 2.4 3.6 4.8 6.0
LDA SCORE (log 10)
C
p=0.001
p=0.01
p=0.05
Lactobacillus
Parabacteroides
Bacteroides acidifaciens
Allobaculum
-log10 FDR p-value
Effect size
Non-responder
Responder
Phylum
Class
Order
Family
Genus
Species
D
Relative abundance of B.acidifaciens
Non-responder
Responder
E
Relative abundance of Bacteroidales S24-7
Non-responder
Responder

Figure 5

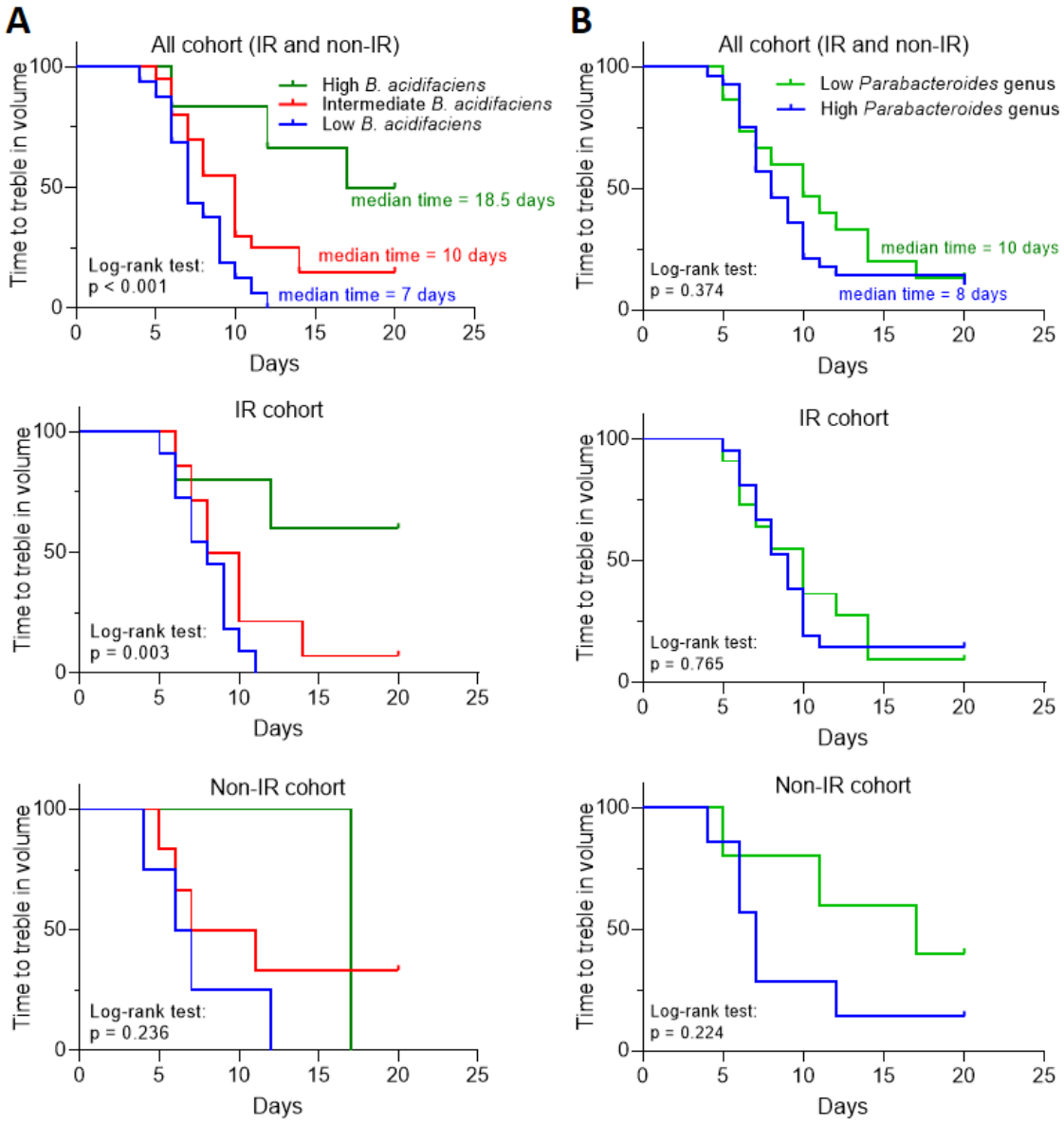
A
All cohort (IR and non-IR)
High B. acidifaciens
Intermediate B. acidifaciens
Low B. acidifaciens
median time = 18.5 days
median time = 10 days
median time = 7 days
Log-rank test:
p < 0.001
Time to treble in volume
Days
IR cohort
Log-rank test:
p = 0.003
Non-IR cohort
Log-rank test:
p = 0.236
B
All cohort (IR and non-IR)
Low Parabacteroides genus
High Parabacteroides genus
median time = 10 days
median time = 8 days
Log-rank test:
p = 0.374
IR cohort
Log-rank test:
p = 0.765
Non-IR cohort
Log-rank test:
p = 0.224

Figure 6

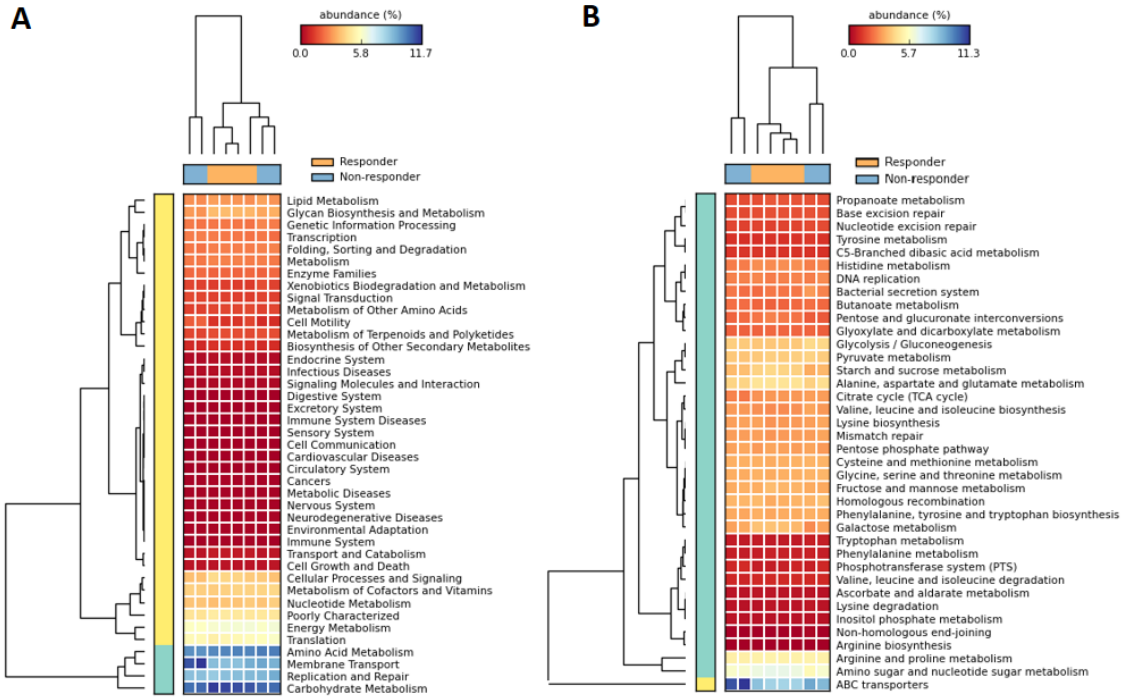
A
abundance (%)
0.0
5.8
11.7
Responder
Non-responder
Lipid Metabolism
Glycan Biosynthesis and Metabolism
Genetic Information Processing
Transcription
Folding, Sorting and Degradation
Metabolism
Enzyme Families
Xenobiotics Biodegradation and Metabolism
Signal Transduction
Metabolism of Other Amino Acids
Cell Motility
Metabolism of Terpenoids and Polyketides
Biosynthesis of Other Secondary Metabolites
Endocrine System
Infectious Diseases
Signaling Molecules and Interaction
Digestive System
Excretory System
Immune System Diseases
Sensory System
Cell Communication
Cardiovascular Diseases
Circulatory System
Cancers
Metabolic Diseases
Nervous System
Neurodegenerative Diseases
Environmental Adaptation
Immune System
Transport and Catabolism
Cell Growth and Death
Cellular Processes and Signaling
Metabolism of Cofactors and Vitamins
Nucleotide Metabolism
Poorly Characterized
Energy Metabolism
Translation
Amino Acid Metabolism
Membrane Transport
Replication and Repair
Carbohydrate Metabolism
B
abundance (%)
0.0
5.7
11.3
Responder
Non-responder
Propanoate metabolism
Base excision repair
Nucleotide excision repair
Tyrosine metabolism
C5-Branched dibasic acid metabolism
Histidine metabolism
DNA replication
Bacterial secretion system
Butanoate metabolism
Pentose and glucuronate interconversions
Glyoxylate and dicarboxylate metabolism
Glycolysis / Gluconeogenesis
Pyruvate metabolism
Starch and sucrose metabolism
Alanine, aspartate and glutamate metabolism
Citrate cycle (TCA cycle)
Valine, leucine and isoleucine biosynthesis
Lysine biosynthesis
Mismatch repair
Pentose phosphate pathway
Cysteine and methionine metabolism
Glycine, serine and threonine metabolism
Fructose and mannose metabolism
Homologous recombination
Phenylalanine, tyrosine and tryptophan biosynthesis
Galactose metabolism
Tryptophan metabolism
Phenylalanine metabolism
Phosphotransferase system (PTS)
Valine, leucine and isoleucine degradation
Ascorbate and aldarate metabolism
Lysine degradation
Inositol phosphate metabolism
Non-homologous end-joining
Arginine biosynthesis
Arginine and proline metabolism
Amino sugar and nucleotide sugar metabolism
ABC transporters

Figure 7